Accepted Manuscript

ARTICLE

A heated rock crack captures and polymerizes primordial DNA and RNA

Christina F. Dirscherl[a], Alan Ianeselli[a], Damla Tetiker[a], Thomas Matreux[a], Robbin M. Queener[a], Christof B. Mast[a] and Dieter Braun[a]*

Life is based on informational polymers such as DNA or RNA. For their polymerization, high concentrations of complex monomer building blocks are required. Therefore, the dilution by diffusion poses a major problem before early life could establish a non-equilibrium of compartmentalization. Here, we explored a natural non-equilibrium habitat to polymerize RNA and DNA. A heat flux across thin rock cracks is shown to accumulate and maintain nucleotides. This boosts the polymerization to RNA and DNA inside the crack. Moreover, the polymers remain localized, aiding both the creation of longer polymers and fostering downstream evolutionary steps. In a closed system, we found single nucleotides concentrate 10^4-fold at the bottom of the crack compared to the top after 24 hours. We detected enhanced polymerization for 2 different activation chemistries: aminoimidazole-activated DNA nucleotides and 2',3'-cyclic RNA nucleotides. The copolymerization of 2',3'-cGMP and 2',3'-cCMP in the thermal pore showed an increased heterogeneity in sequence composition compared to isothermal drying. Finite element models unravelled the combined polymerization and accumulation kinetics and indicated that the escape of the nucleotides from such a crack is negligible over a time span of years. The thermal non-equilibrium habitat establishes a cell-like compartment that actively accumulates nucleotides for polymerization and traps the resulting oligomers. We argue that the setting creates a pre-cellular non-equilibrium steady state for the first steps of molecular evolution.

Introduction

A fundamental question of biology is how life originated on early Earth. A plausible hypothesis uses RNA oligomers to start molecular evolution [1]. This is founded in the fact that they can act both as information storing and catalytic molecules. The formation of the individual mononucleotides has been extensively studied recently [2-6] under lab conditions using high starting concentrations. However, functional RNA, just like DNA, are large macromolecules and their autonomous prebiotic formation from single nucleotides remains a fundamental problem. Chemical mechanisms have been found that enable de novo strand formation from activated RNA monomers [7-9]: imidazole-activated RNA molecules [10-13] and 2',3'-cyclic monomers [9,14,15].

The formation of oligonucleotides requires high starting concentrations. How these high concentrations can be provided and how the products can be prevented to be diluted by diffusion remains largely unclear. In order to obtain a persistent pool of informational macromolecules such as RNA or DNA, their formation from monomeric building blocks must outpace their destruction and their removal by diffusion. Here we studied how the physical characteristics of thermogravitational pores would have provided a suitable environment.

We studied two prebiotically relevant polymerization chemistries (Fig. 1b). Previously, Orgel [10], Ferris [11], McGown [12] and others [13] have shown that the preactivation of monomers with imidazoles triggers the oligomerization of short RNA molecules. We here used such an imidazole activation for the polymerization of more stable DNA nucleotides in aqueous solution. DNA nucleotides have been shown in other works [4-6] to form under relevant conditions and have been hypothesized to consequently have evolved at an early stage. The other polymerization chemistry of this study uses 2',3'-cyclic RNA nucleotides [9,14,15], with experimental protocols based on previous experiments using 3',5'-cyclic GMP [16,17]. The polymerization of 2',3'-cyclic RNA nucleotides takes place under dry conditions at elevated pH. However, both polymerization chemistries usually require high concentrations of starting material. Furthermore, like all chemical systems, they naturally relax into their thermodynamic equilibrium destroying longer polymers, erasing all reached complexity. The question of under what environmental conditions RNA could evolve into complex informational macromolecules therefore remains an important hurdle.

Our experiments suggest that heat fluxes from a physical non-equilibrium could have tipped the balance in favor for complexity. Equilibrium settings usually lack a directed accumulation process to transport molecules towards a spatially localized setting. Compartmentalized systems such as vesicles or coacervates in published cases were shown to trade localization of molecules for a reduced reactivity [18,19]. Heat fluxes across water-filled rock cracks and pores are considered a ubiquitous setting on early Earth [20,21]. In laboratory conditions, it was previously shown that mimics of such water-filled cracks exposed to thermal gradients drive

a. *Systems Biophysics and Center for NanoScience, Ludwig-Maximilians-Universität München, 80799 Munich, Germany*
* Corresponding Author: dieter.braun@lmu.de

thermogravitational accumulation of DNA polymers [22]. This is induced by the physical non-equilibrium of thermal gradients that generates convection and thermophoresis (the directed movement of molecules along a thermal gradient) inside the pore, causing strong accumulation of dissolved molecules towards the pore bottom for a range of different geometries and thermal gradients [23-28].

In our experiments, such pores actively collect and concentrate the monomeric RNA and DNA starting material, overcoming its high diffusivity (~$0.75*10^5$ cm^2/s, [29]) without restricting their reactivity. In addition, the polymerized products are retained at the bottom of the pore while fresh monomers can be supplied from the top of the pore without diluting the reaction mixture at the bottom. This provides an effective decoupling of the feeding of solutes from the addition of solvent. This contrasts with other mechanisms such as simple addition of new volumes of starting material where feeding fresh reactants is accompanied by dilution of the already polymerized products [30] as is the case for example in tidal pools. In the water-filled pore, we found an enhancement of up to 300 % for the polymerization of imidazole-activated DNA nucleotides.

Liquid filled rock pores can contain gas bubbles, for example in settings close to the surface or due to degassing. When a gas bubble is trapped inside a pore, microscale wet-dry cycles take place at the air-water interface [31,32] (Fig. 1a). Macroscopic wet-dry cycles, like for example evaporative lakes [33-35], loose water through evaporation but are rehydrated with buffers in forms of rivers, splashes and rain from larger reservoirs. As seen also on modern Earth [36], this can lead to runaway salt concentrations and large pH shifts [37]. A heated pore with an air inclusion however provides a closed system with microscale wet-dry cycles: water evaporates on the warm side and reenters as dew droplets at the cold side. This prevents a global change of salt concentration. Here, we show that such a system can drive polymerization reactions that require dry conditions. The yield was enhanced due to both, the accumulation properties of a thermophoretic pore and the constant wet-dry cycling while the pH and salt conditions were kept stable by the wet system. The conditions in this study couple water-based accumulation by thermophoresis to the wet-dry cycles at a gas bubble in a thermal pore. This enables the molecules to shuttle in a short time between the wet and the dry environment, allowing reactions in both media in parallel [31,32].

Our work suggests a setting in which prebiotic molecules could have become sufficiently concentrated to trigger an efficient polymerization of nucleotides into longer sequences of increased complexity. Once created, thermophoresis would keep the formed polymers in place over prolonged periods of time and allow for the resupply of starting material without dilution.

Results and Discussion

A. Monomer Accumulation Studies on oligonucleotide polymerization started from high mononucleotide concentrations [7,11,15] with up to 200 mM to facilitate de novo strand polymerization. On early Earth, it is far from obvious what

environments could have provided such high monomer concentrations, commonly called the concentration problem [38,39].

Thermal gradients across a confined water pocket induce two physical phenomena. The bulk solution undergoes a circular convection motion due to the heat-induced density differences within the liquid. Also, the dissolved molecules experience thermophoresis, a drift along the temperature gradient. For charged molecules such as DNA or RNA this effect is most pronounced and moves them vertically to the colder side of the pore [40,41]. The superposition of both effects leads to an exponential concentration increase of molecules at the bottom of the pore (Fig. 1). The resulting accumulation of molecules is balanced by diffusion, seeking a homogeneous concentration. In the steady state the concentration distribution inside the pore can be described by [25,42,43]

$$\frac{c_{bot}(h)}{c_{top}} \propto exp(S_T\, r\, \Delta T), \text{ with } r = h/w \tag{1}$$

where $c_{bot}(h)$ is the concentration at the bottom of a pore with height h and width w, giving an aspect ratio of r = h/w. $S_T = D_T/D$ is the Soret coefficient of the molecules, D_T the thermodiffusion coefficient, D the ordinary diffusion coefficient, ΔT the applied temperature difference across the width of the pore.

To experimentally implement this non-equilibrium setting, we cut out the microfluidic structure from a Teflon foil with 170 µm width, that is sandwiched between two thermally conducting sapphire plates. We applied cooling by a waterbath on one side and Ohmic heating on the other side (see Fig. 1c and SI-Section II). The pore was filled with unactivated 2.5 mM, 20 mM or 300 mM dAMP DNA-mononucleotides in 100 mM MOPS buffer. The accumulation was visualized in realtime by low concentrations of fluorescent Cy5 molecules which co-accumulate with the DNA (Fig. 1d and SI-Movie S5). The content of the pore was extracted after 24 h in individual sections along its height by quick freezing, cutting and subsequent extraction in separate volume sections (SI-Section III).

The local concentration of molecules in each section was then measured with HPLC-MS (SI-Sections IV-VI). Fig. 1e shows that after a runtime of 24 h an up to 10-fold absolute accumulation of dAMP monomers was achieved at the bottom of the pore compared to the starting concentration. The top concentration depleted simultaneously, yielding an about 10^4-fold relative accumulation. The accumulation did not depend on the starting concentration, as expected from the general finding that thermophoretic properties only depend on the molecule concentration in highly crowded conditions [40,44]. A finite element simulation combined heat transfer, fluid convection, molecule diffusion and thermophoresis in a 2D model of the crack (Fig. 1e, solid lines, SI-Section IX), showing good agreement with the experimental data (circles). RNA has very similar thermophoretic properties and thus is expected to behave very similarly [40,45].

Heated rock pores on the volcanic, early Earth were likely ubiquitous in a wide range of shapes and sizes and were subjected to very different temperature conditions. Even if heated with much more shallow thermal gradients, a similar but slower accumulation is expected [27,29]. Our experimental settings were optimized for fast

accumulation, accepting a rather steep thermal gradient. The robustness of molecule accumulation, however, was mapped out for different temperature gradients ($\Delta T = 5 - 50°C$) and pore widths (200 µm – 400 µm) in SI-Fig. 12. This geometrical versatility provides a wide range of possible rocky environments where temperature gradients could have helped in the concentration and dilution problem on early Earth.

B. DNA Polymerization De novo strand polymerization of imidazolize-activated RNA and DNA nucleotides has been studied under various conditions before and was found to proceed in aqueous state with all four bases[13,46,47]. This is the reason to implement this reaction only for Adenosine as the thermal trap enhances the concentration and does not rely on drying the nucleotides as later studied for 2'3'-cyclic G and C. We applied this scheme to DNA monomers and found DNA oligomerization in water (see Fig. 2 and SI-Fig. 14). Activated 2'-aminoimidazole dAMP monomers (AImpdA) at concentrations of 2.5, 20 or 300 mM in 100 mM MOPS buffer at pH 6.5 were incubated under homogeneous temperature of 8°C or 30°C in bulk or exposed to the thermal gradient of $\Delta T = 30°C - 8°C = 22°C$ in the pore for 24 h. The reaction was stopped by freezing. The contents of the pore were again extracted in individual sections along its height.

The mass spectrometry revealed three different types of products (Fig. 2a): (i) linear oligomers in which all bonds are 3',5'-phosphodiester bonds, (ii) activated oligomers which are linear oligomers that still have the aminoimidazole activation-group at the 5'-end and (iii) pyrophosphate oligomers in which exactly one monomer linkage is a pyrophosphate bond (the rest are 3',5'-phosphodiester bonds). Obtaining heterogeneous backbones with pyrophosphate linkages should not be detrimental, arguing along the lines of [48] that DNA pyrophosphate linkages stabilize the base pairing of mixed DNA-RNA duplexes. The incorporation of 2'-5' linkages into a strand has been shown by [53, 54] to lower the melting temperature of oligomers which is critical for the replication of sequences. The same studies show that 2'-5' linkages are not opposing the development of functional RNA as they still allow for 3D RNA folding. Additionally, 2'-5' linkages are more prone to hydrolysis, hence in a wet-dry cyclic environment automatically the 3'-5' linkages could be selected over the 2'-5' ones [53,55,56].

The combined HPLC-MS analysis allowed us to quantify the different types of oligomerization products for each oligomer length (SI-Sections V-VI). No cyclic oligomer products were detected.

The results are shown in Figure 2b. We found up to 4mers for pyrophosphate and activated oligomers, linear oligomers formed up to a length of 3nt. The non-equilibrium accumulation behavior of the pore enhanced the efficiency of oligomerization up to 24-fold compared to the bulk experiments (SI-Fig. 16) for all three different types of oligomers. The finite element simulation of accumulation and polymerization was consistent with the experimental observations (Fig 2b, lines and markers).

Polymerization of AImpdA occurred throughout the whole chamber volume but was enhanced nonlinearly by the increased monomer concentration at the bottom. Monomers and polymers were

similarly accumulated by the heat flow condition. After 24 h and without additional feeding, about 30 % of the oligomerization products still had their aminoimidazole activation group. If fed from the top of the pore via connecting to a large reservoir and if run over larger time scales, the polymerization is expected to continue since thermophoresis efficiently prevents monomers and oligomers from leaving the thermal chamber as can be seen in the theoretical simulations below.

C. RNA Polymerization When gas bubbles are added into the heat flow, it was recently shown that DNA and RNA strands accumulate [32], phosphorylate [31] and enzymatically polymerize [49] by the created local wet-dry cycles. At the gas-water interface of the bubble, the combination of capillary forces and surface tension drives a continuous coffee-ring effect [50,51]. If driven by a polymerase, the setting was found to yield up to 1300 base long DNA sequences [48]. For RNA, we studied the recently established polymerization from 2',3'-cyclic RNA monomers [14]. This chemistry was studied in the past for AMP with the help of various catalysts [9,15]. Only recently, it was found that 2',3'-cGMP itself can trigger oligomerization in the dry at elevated pH without ions or added catalysts [14], then leading the way to copolymerization with other bases. Possibly aided by the G-base in a yet unknown stacking arrangement, the 5'-hydroxyl attacks the 2',3'-cyclic phosphate and leads to the opening of the phosphate ring either at the 2'- or the 3'-oxygen of the sugar. The product is an oligomer with 2',5'- or 3',5'-phosphodiester bonds and either an open (3'-P or 2'-P) or closed (2',3'-cP) phosphate ring (Fig. 3a). Both cyclic and linear phosphate endings were analyzed independently, but displayed as a sum in the graphs for simplicity. The aim was to demonstrate how the wet-dry polymerization of an air-water interface can be combined with the upconcentration of a thermophoretic chamber to enhance the de novo dry polymerization of RNA from 2',3'-cyclic nucleotides

For this purpose, a gas bubble was introduced at the bottom of the pore. Convection and thermophoresis were now joined by local evaporation and recondensation at the gas-water interface. In addition to the downward accumulation, this induces a wet-dry cycling of the solutes. RNA molecules deposited in layers on the warm side (Fig. 1a, photo) and rehydrated by growing dew droplets from the cold side, re-entering the fluid phase and oscillating the vertical position of the water-air interface over time (SI-Movie S6).

For the experiment, 10 mM 2',3'-cyclicGMP and 50 mM 2',3'-cyclicCMP were dissolved in RNAse-free water and the pH was adjusted to pH 10.5 with KOH. The higher concentration of C reflects its higher solubility and compensates for a reduced reactivity in the copolymerization. The mixture was inserted in the heated pore, leaving a gas bubble at the bottom (SI-Movie S2). We then applied a thermal gradient of $\Delta T = 70°C - 40°C = 30°C$ for 18 h (SI-Section II). As comparison, 20 µl of the mixture were incubated in test tubes for 18 h at 40°C or 70°C with the tube lid open to induce dry conditions or closed to probe aqueous-only conditions. After 18 h of reaction, the dried tube samples were rehydrated into 20 µl of RNAse-free water and all tubes and the pore were frozen at -80°C to stop the reaction. The pore sample was again cut and extracted in individual volume sections along the pore height. The oligomer concentrations

were measured with HPLC and ESI-TOF after ethanol precipitation (see SI-Section III).

A direct comparison between the reaction at the pore bottom versus the control experiments in the test tubes showed that the thermal non-equilibrium pore triggered the formation of a 3-fold higher yield and 1-2 nt longer oligomers, despite the fact that only a very small fraction near the bottom bubble of the pore volume was drying (Fig. 3b, circles). 7mers could be detected at the pore bottom while only 5mers and 6mers were found in the bulk drying experiments at isothermal conditions. The bulk control without any drying merely yielded 4mers. One should consider that at the bottom of the chamber drying conditions were implemented only by the air bubble while in the dry sample the full volume has been dried. In contrast to the drying conditions, the thermophoretic pore can confine the monomeric starting material and the oligomer product at the air-water interface by the combined thermophoresis and convection. Hence, the relative yield per volume is considerably higher in the crack.

The observations could be rationalized in detail by a combined accumulation and polymerization simulation (Fig. 3b and c, solid lines, SI-Section IX) where the polymerization was implemented only in a small section near the bottom of the chamber representing the water-air interface of the pore. As shown in [31], the polymerization process of 2',3'-cyclic monomers strongly depends on the efficient stacking of the 2',3'-cGMP. Pure G-strands were the dominant species, despite the initial 1:5 concentration bias towards cCMP since cCMP has a lower probability for incorporation. Interestingly, the non-equilibrium setting was able to increase the incorporation efficiency of 2',3'cCMP into the oligomers compared to the dry polymerization (up to doubling it, see inset of Fig. 3c) regardless of the initial monomer concentrations or the initial G/C ratios (1:5, 2:2, 10:50, 20:20, also see SI-Fig. 15). It should be noted that cCMP shows a much higher solubility than cGMP. Therefore, since the trap accumulates cGMP and cCMP comparably, we expect that in the pore also the cCMP is accumulated near its solubility limit, leading to a dried state with a significant higher concentration ratio of C to G in the dry state, naturally compensating for the lower oligomerization rate of cCMP.

The highest 24-fold enhancement of polymerization was seen at the lowest G-concentration experiment that starts with 1 mM cGMP and 5 mM cCMP (Fig. 3d), indicating again that the up-concentration by thermophoresis is limited by solubility for the higher concentrations. The polymerization dynamics is as expected nonlinear: the rate limiting, slow formation of dimers with an effective dimerization rate equation of $k_{11}^{eff} * (c_{mono})^2$ is suggested by the numerical polymerization model. Therefore, dimer concentrations are expected to scale quadratically with the initial concentration of 2',3'-cGMP. This is confirmed in the data in Figure 3e. The fitted $k_{11}^{eff} = 5.7 \pm 0.1 * 10^{-5} (Ms)^{-1}$, is about one order of magnitude higher than what is needed to fit the polymerization in the microscopic model in Figure 3c that includes thermophoresis. The higher effective rate shows in a nutshell the efficient enhancement of polymerization by the heated crack already for the short experimental time of 18h.

With the above results, we can conclude that the non-equilibrium setting yielded longer strands and increased concentrations with a more balanced, mixed base composition. This is expected to make the sequences more likely to hybridize with each other, offering an increasingly likely pathway towards downstream evolutionary reactions such replication by templated ligation.

D. Numerical Simulations for Long Timescales We used a finite element simulation to extrapolate the 2',3'-cyclic RNA polymerization reaction experimental results to timescales not yet accessible for lab experiments (SI-Section IX.5). We first explored how offering a low concentration of 1μM of monomers at the top of the crack leads to long term accumulation (Figure 4a). This is however a slow process and simulations of other settings, for example a flow through the whole chamber [26,52], show that the kinetics of filling the chamber from the top is actually the worst case scenario in terms of time required. If fed from top, it would take significantly longer than a year to completely fill the crack of our experiment (solid line).

But feeding from top does offer a near perfect retention of the already accumulated molecules. Even if the feeding from the top would stop after a year, none of the molecules escape over the time scale of many years (Figure 4a, broken line). This is especially interesting for the polymerization reaction whose informational polymers are kept in place for long times and have ample time to recycle and react along complex evolutionary pathways without being lost by diffusion. In terms of concentration distribution, one can compare the exponential distribution in the centimeter-long crack with how Earth is able to keep its kilometer-high gas atmosphere over long times by gravity.

We studied the filling of the pore over time in this scenario in Figure 4b. When it is not fed, as in our experiments, the accumulation at the bottom creates a depletion at its top (Fig. 4b, broken lines). While the monomer accumulation is 10-fold compared to the starting concentration within 24 h in our experiments at the bottom, a longtime two-dimensional simulation shows that only the bottom fifth of the chamber is required for this 10-fold accumulation. The top of the chamber depleted 10^6-fold for the closed pore.

But if we connect the top to an outside reservoir of a low concentration of 1 μM, the chamber has the potential to slowly build up a 10^6-fold accumulation, however at a rate of only 0.6μM/s as inferred from the 2D pore simulation of Figure 4a. The notable point is that this feeding adds fresh starting material without the addition of bulk water and hence without the dilution of already formed products. This is a unique characteristic of this form of a heated rock pore setting.

We studied how above's feeding and accumulation would be able to overcome the natural enemy of RNA polymerization: hydrolysis. Into our 2',3'-cyclic polymerization simulation, we included the deactivation of active 2',3'-cyclic monomers with a rate of 1/day to 2' or 3' phosphate monomers which do not polymerize. In the long-time simulation now, we also included the hydrolysis of the oligomer backbone which was only possible in a 0D simulation. The simulation was fed with 0.6 μM/s inferred from the 2D simulation and the

polymerization rates were slightly tuned to match the results of Figure 3c (SI-Section IX.5). This allowed us for all GC-mers up to 21mers to be sure that polymers up to half of this length are correctly tracked.

With this, we studied the hydrolysis of the strands into inactive 2' or 3' phosphates at a rate of 1/(2 days) (Figure 4c) or 1/(90 days) (Figure 4d) to estimate a range of possible hydrolysis rates. To aim for a worst case, we neglected the possible hydrolysis into active 2',3'-cyclic ended oligomers. The rate equations were generated with a LabView program (2.2 MB text file, see Dataset S6, SI-Section XII) and interestingly could be solved by Comsol Multiphysics (see Dataset S6, SI-Section XII) in less than a minute on a normal notebook.

Without feeding, the polymerization succumbed in the long run to the hydrolysis channels (broken lines), leaving not much RNA after a year. But already feeding at the moderate 1 µM lead to long RNA at very high concentrations (solid lines), likely leading to precipitation or gelation of the generated strands. This shows that the accumulation and polymerization in a thermal gradient is an ideal combination as we inferred already a while ago in another study [22].

Unfortunately, leakages of the microfluidics setups still prevent such experiments. However the simulations show that experiments run slightly longer, boosted for example by allowing a higher top concentration (feeding), will likely lead to very interesting results using the heated rock pore with an air-bubble at the bottom. We hope that optimizations of the system will allow such experiments in the near future.

Conclusions

Our study demonstrates how physical non-equilibria can enhance prebiotically relevant chemical reactions by concentrating and actively confining biomolecules. The experiments explored the link between the phosphorylation of nucleosides [17] and the replication triggered by strand separation towards longer strands [18,49], found for heated air-water interfaces. In contrast to equilibrium settings, the accumulation in a thermophoretic pore avoids the need for high starting concentrations of DNA/RNA monomers. Even more importantly, the heat flux prevents the diffusional dilution of polymerization products after their creation and maintains the information over time scales only set by the geological heat flow itself.

The feeding of the polymerization reaction is simple: monomeric molecules at low concentrations are offered at the top of the crack, are added and accumulated continuously to the reaction at the bottom, enabling a long-term setting for reactions with informational molecules. The polymerization in the heat flow for RNA was found to create sequences with a more balanced G/C composition, approaching the ability to base pair and increasing the sequence space encoded by the strands. We found that by exploiting this thermal non-equilibrium in a thin crack, a rich and localized pool of oligomers with a diverse sequence composition was created in the experiments. On early Earth this would have facilitated the first steps towards starting a minimal form of molecular evolution.

Materials and Methods

AImpdA Synthesis 3.3 mmole (1 eq) deoxythymidine-5'-monophosphate disodium salt (dTMPNa$_2$, CAS No. 33430-62-5, Carbosynth Ltd.) and 16.4 mmole (5 eq) 2-aminoimidazole sulfate salt (SKU No. 197912-2.5G, Sigma Aldrich) were dissolved in 25 mL of RNAse free water (Ambion TM Nuclease-Free Water, Ref. No. AM 9932, Life Technologies Corporation) in a 50 mL polypropylene Falcon tube. The pH was adjusted to 5.7 by adding a solution of syringe-filtered 1 M hydrogen chloride (HCl, Art. No. K025.1, Carl Roth GmbH + Co. KG). RNAse free water was added to give a total volume of 30 mL. The mixture was filtered with a 0.45 µm filter and aliquoted into two 50 mL polypropylene Falcon tubes, flash-frozen in liquid nitrogen, and lyophilized for two days. In 250 mL glass round-bottom flasks, a mixture of 50 mL anhydrous dimethyl sulfoxide (SKU No. 276855-1L, Sigma-Aldrich) and 6.2 mL anhydrous triethylamine (CAS No. 121-44-8, Carl Roth GmbH + Co. KG) was stirred under argon. The lyophilized products were added and heated gently in a flame for 30 min. To each flask, 29.5 mmole (9 eq) triphenylphosphine (TEA, CAS No. 603-35-0, Carl Roth GmbH + Co. KG COMPANY) and 32.8 mmole (10 eq) 2,2'-dipyridyldisulfide (SKU No. 8411090005, Sigma-Aldrich) were added. The mixtures were stirred under argon for 30 min. The solutions were poured in an ice-cooled glass bottle containing a mixture of 400 mL acetone (UN No. 1019, Carl Roth GmbH + Co. KG), 250 mL diethyl ether (CAS No. 60-29-7 Carl Roth GmbH + Co. KG company), 30 mL trimethylamine (UN No. 1296, Carl Roth GmbH + Co. KG) and 1.6 mL acetone saturated with natriumperchlorat (NaClO$_4$) (SKU No. 410241-500G, Sigma-Aldrich), and stirred until the product flocculated. Stirring was stopped and the bottle was put on ice for 30 min. The solution was collected in 50 mL propylene Falcon tubes and centrifuged at 4000 rpm for 3 min at 10°C. The supernatant was discarded and the pellets were resuspended in 10 mL of a 1:8.3:13.3 of triethylamine:diethyl ether:aceton mixture. The new solutions were vortexed and centrifuged at 4000 rpm for 3 min at 10°C. The supernatant was discarded, and the step was repeated. The pellet was washed twice with 10 mL acetone and twice with 10 mL diethyl ether. The pellets were dried overnight under vacuum. The product was stored at -20°C.

dAMP Accumulation Deoxyadenosine-5'-monophosphate disodium salt (dAMPNa2, CAS No. 2922-74-9, Carbosynth Ltd.) powder was allowed to thaw to room temperature, weighed into a low-binding test tube and mixed with a 100 mM 3-(N-morpholino)propanesulfonic acid (MOPS) buffer solution to the desired concentration (300 mM, 20 mM, 2.5 mM). The pH naturally settled at pH 6.5. The sample mixture was filled into a thermophoretic pore, which had beforehand been filled with low viscosity oil (3M TM Novec TM 7500, IoLiTec Ionic Liquids Technologies GmbH) to allow complete filling of the pore without introducing any air bubbles. The pore was operated for 24 h at a temperature gradient of ΔT = 22°C, with the hot temperature at 30°C and the cold temperature at 8°C at the front and back of the solution.

AImpdA Polymerization Self-synthesized AImpdA powder was prepared for experiments as dAMP in the section before. The pore

ARTICLE

was operated for 24 h at a temperature gradient of $\Delta T = 22°C$, with $T_{hot} = 30$ C and $T_{cold} = 8°C$. For the bulk controls, 20 µl of sample was filled in Eppendorf test tubes and covered with 15 µl of paraffin oil (Art. No. 9190.1, Carl Roth GmbH + Co. KG) to prevent any evaporation inside the test tube. The tubes were incubated for 24 h at 30°C and 8°C, respectively.

2',3'-cyclic Polymerization 2'3'cCMP (Na-salt form, CAS No. 15718-51-1, Sigma-Aldrich) and 2'3'cGMP (Na-salt form, Cat. No. G025-50, Biolog Life Science Institute GmbH & Co. KG) were mixed with RNAse free water to the desired concentrations and G/C ratios (10 mM/50 mM, 1 mM/5 mM, 20 mM/20 mM, 2 mM/2 mM). The pH of the solution was adjusted to 10.5 with potassium hydroxide (KOH, Art. No. K017.1, Carl Roth GmbH + Co. KG). If visualization of the accumulation process was desired, 10 µM Cy5 fluorescent dye (Cat. 23390, Lumiprobe GmbH, excitation maximum: 649 nm, emission maximum: 666 nm) were added, which was tested in a separate experiment not to change the polymerization behavior. The sample mixture was filled into an air-filled thermophoretic pore from its top until it filled the upper 4/5 of the chamber volume, the lowest fifth was left air-filled to create the liquid-gas interface. The filling procedure with an air-water interface is shown in SI-Movie S2. The pore was operated for 18 h at a temperature gradient of $\Delta T = 30°C$, with the hot temperature at 70°C and the cold temperature at 40°C. For the dry control, 20 µl of the sample was filled in test tubes and incubated for 18 h at 40°C and 70°C, respectively, with the tube lid open to allow evaporation. After the 18 h, samples were rehydrated with 20 µl of RNAse free water. For bulk controls, 20 µl of sample was filled in test tubes and covered with 15 µl of low viscosity paraffin oil (CAS No. 8042-47-5, Carl Roth GmbH + Co. KG) to prevent any evaporation inside the test tube. The tubes were kept with closed lids for 18 h at 40°C and 70°C, respectively.

Pyrophosphatase Enzyme Digestion Protocol We used the NudC Pyrophosphatase Kit (M0607S, New England BioLabs Inc.) for digestion of pyrophosphate-linkages in our AImpdA-polymerization products. After 24 h of incubation at 20°C in a test tube, 15 µl of a 2.5mM-AImpdA sample were mixed in a new test tube with the following chemicals, all included in the kit: 2 µl NEBuffer 3.1 (10x), 1 µl 100 mM DTT (dithiothreitol) and 2 µl NudC pyrophosphatase (10 µM). The tube was vortexed, spun down and incubated for either 1 h or 2 h at 37°C. Without further treatment, we measured the digested sample with the same HPLC-MS protocol as the undigested sample and compared the results of both measurements. Data and analysis are shown in SI-Fig. 1 and SI-Tab. 1.

Microfluidic Chamber and Experimental Setup The non-equilibrium experiments were performed in a chamber (170 µm × 7 mm × 52 mm, total volume: 62 µl) cut from a thin Teflon foil (170 µm thickness, FEP-Teflon, Holscot, Netherlands) and was placed between a transparent cooled back sapphire of 0.5 mm thickness (with four laser-cut holes of 1 mm diameter, Kyburz, Switzerland) and a heated front sapphire of 2 mm thickness (no holes, Kyburz, Switzerland). The shape of the Teflon foil was designed in Inventor (Autodesk) and cut with a cutting plotter (CE6000-40 Plus, Graphtec). The sapphires were lined with two heat-conducting graphite foils (one of 25 µm thickness in the back, EYGS091203DP,

1600 W/mK, Panasonic, one of 200 µm thickness in the front, EYGS0811ZLGH, 400 W/mK, Panasonic) to ensure a good thermal connection to an aluminum plate at the back and to the resistance rod heaters at the front. The layers were screwed together with a steel frame. This sandwich is screwed to a waterbath-cooled (TXF200, Grant Instruments (Cambrigde) Ltd) second aluminum block with another 200 µm thick graphite foil in between. Four microfluidic inlet-/outlet teflon tubings (KAP 100.969, Techlab) were connected with fittings and ferrules (VBM 100. 823 and VBM 100.632, Techlab) to the sapphire back wall of the chamber, which has four holes of 1 mm diameter. For the dAMP and the AImpdA experiments, the waterbath (50/50 water/ethylene-glycol) was set to -30°C and the resistance heaters to 80°C. For the 2'3'cyclic experiments, the waterbath was set to -20°C and the resistance heaters to 100°C. To calculate the inner temperatures of the chambers, we measured the temperatures on the outside of the sapphires with a temperature sensor (GTF 300, Greisinger) and a thermometer (GTH 1170 Typ K, Greisinger) and used the steady-state linear heat equation and the conductivities of water 0.60 W/mK (at 20°C) and sapphire 23 W/mK to calculate what temperature this translates to on the inside of the pore. The fluorescent microscopy setup consisted of a standard fluorescence microscope (Axiotec, Carl Zeiss Microscopy Deutschland GmbH) equipped with an LED (622 nm, ThorLabs), a dual excitation filter (470 nm/622 nm), a dual emission filter (537 nm/694 nm), a dual band beamsplitter (497 nm/655 nm), a 2x objective (TL2x-SAP, 2x/0.1/350-700 nm/inf/WD 56.3 mm, ThorLabs) and a Stingray-F145B ASG camera (ALLIED Vision Technologies Gmbh). A self-coded program using the software LabVIEW was used to control the camera and the output voltage to the LED and to the resistance heaters.

Freeze Extraction and Sample Preparation We developed a method to differentially extract all sections of the concentration gradient. After the run time of the reaction in the thermal gradient, we turned off the front heating, which lead to a rapid drop in temperature and finally to freezing of the pore contents as the waterbath was maintained at -30°C. After verifying by microscopy that the liquid contents were frozen, we removed the entire pore from the setup and placed it in the -80°C freezer for 30 min and unscrewed the sapphire-teflon-sapphire sandwich from the metal holders. The sandwich was placed on an aluminum block cooled to -80°C to prevent melting. The sandwich was opened, the frozen liquid content was cut into five sections (for experiments of Fig. 1 and Fig. 2) or three sections (for experiments of Fig. 3) of similar volume. Then the sapphire with the frozen sample on it was slid stripe by stripe over onto a 45°C aluminum block to melt and recover the frozen sample stripe by stripe. After completion of the freeze extraction, the tubes were briefly centrifuged, their liquid contents were weighed, and the percentage of volume to the total extracted volume of the pore was calculated. Then, the pH of the samples was measured with Orion VersaStar Pro pH-meter (ThermoFisher Scientific). We verified that the freezing process did not disturb the accumulation state of the pore by measurements with fluorescent Cy5-dye (SI-Fig. 5). For the experiments of Fig. 1 and Fig. 2, the samples were injected directly into the HPLC-MS system without further treatment. For the experiments of Fig. 3, the samples were precipitated prior to measurement. For the precipitation, 10 µl of sample was mixed with

Journal Name

ARTICLE

90 μl RNAse free H2O, 2 μl of 10 mg/ml glycogen from oyster (G8751-5G, Sigma-Aldrich) and 10 μl of 5 M Ammonium acetate (CAS 631-61-8, Sigma-Aldrich), then vortexed and spun down. 336 μl of - 20°C cold ethanol (Art-Nr. 5054.2, Carl Roth GmbH + Co. KG) was added, the mixture was vortexed, spun down and stored overnight in a 4°C fridge. The next day, the reaction tubes were centrifuged at 15000 rpm for 30 min at 4°C, the supernatant was discarded. 100 μl of -20°C cold 70/30 ethanol/RNAse free water mixture were added. The tubes were centrifuged again at 15000 rpm for 30 min at 4°C. The supernatant was pipetted off as thoroughly as possible and without further drying the pellet was then dissolved in 40 μl of RNAse-free water. With commercial standards over three orders of magnitude and for oligomer lengths from 2 nt to 10 nt we verified that the precipitation did not disturb the composition of the sample (SI-Fig. 6).

HPLC-MS Measurement Methods The HPLC-MS measurements were performed using a time-of-flight mass spectrometer (TOF-MS) with an electrospray ion source (G6230BA, Agilent Technologies) and a 1260 Infinity II Bioinert high performance liquid chomatograph (HPLC, G5654A, Agilent Technologies). The column was an AdvancedBio Oligonucleotides column (4.6 × 150 mm, 2.7 Micron, P.N. 653950-702, Agilent Technologies) and the MS measurements were run in negative mode. For the liquid phase we used as eluent A: UHPLC-water (CAS No. 7732-18-5, Supelco, Merck KGaA) with 200 mM 1,1,1,3,3,3-Hexafluor-2-propanol (HFIP, Art-Nr 2473.3, Carl Roth GmbH + Co. KG) and 8 mM TEA (CAS No. 603-35-0, Carl Roth GmbH + Co. KG COMPANY) and eluent B: 50/50 UHPLC-water/methanol (CAS-No 67-56-1, Merck KGaA) with 200 mM HFIP and 8 mM TEA. After measurement, the masses of the polymerization products were extracted from the raw MS data. We extracted the mass of the most abundant isotope of the molecule, calculated with the Agilent Isotope Distribution Calculator (mass lists and chemical formulas of the polymerization products, see SI-Chapter VI). For the ion extraction algorithm, we tolerated a symmetric margin of error of $\Delta m/z = \pm 2.0$ ppm around the target m/z values. Peak identification for integration was performed by comparing the peaks of the sample with peaks from commercially available standards, enzyme digestion protocol, or hydrolysis experiments. We additionally verified that the selected peaks corresponded to the correct molecule by checking the isotope distribution signature of the peak in the first charge state. The selected peaks were integrated and the background was subtracted either manually using the MassHunter Qualitative Analysis program or with a self-coded LabVIEW program. To retrieve the concentration information from the integrated peak areas, a calibration procedure was used, which is described in SI-Section V.

dAMP Accumulation: The injection volume was 2 μl for each sample, and the compressibility was set to $40*10^{-6}$ L/bar. A flow of 0.6 ml/min was maintained throughout the 40 min of the method. The column temperature was 30°C and the eluent gradients were 0.0 min: 79.0 % A 21.0 % B, 23.00 min: 53. % A 47.0 % B, 23.1 min: 0.0 % A 100.0 % B, 30.0 min: 0.0 % A 100.0 % B, 30.1 min: 79.0 % A 21.0 % B, 40.0 min: 79.0 % A 21.0 % B. The recorded diode array detector (DAD) signal was set to 259 nm with a bandwidth of 4 nm. The measured mass range (m/z) was 320 u – 3200 u with a scan rate of 3 spectra/sec. The settings were: sheath gas flow: 11 L/min,

sheath gas temperature: 400°C, nebulizer: 45 psig, gas flow: 5 L/min, gas temperature: 325°C, octupole RF-peak: 800 V, skimmer: 65 V, fragmentor: 250 V, nozzle: 2000 V, V-cap: 4000 V. The reference masses were 1033.988109 u and 1333.968947 u (commercially available from Agilent).

AImpdA Polymerization: The method was almost the same as for the dAMP accumulation experiments, except for the mass range, which excluded the monomer masses to obtain a cleaner ion chromatogram with lower background: mass range 550 u – 3200 u. Other minor changes were the gas flow: and the gas temperature: 300°C.

2',3'-cyclic Polymerization: The injection volume was 38 μl for each sample, and the compressibility was set to $50*10^{-6}$ L/bar. A flow of 1.0 ml/min was maintained throughout the 53 min of the method. The column temperature was 60°C and the eluent gradients were 0.0 min: 99.0 % A 1.0 % B, 5.0 min: 99.0 % A 1.0 % B, 27.5 min: 70.0 % A 30.0 % B, 42.5 min: 60.0 % A 40.0 % B, 42.6 min: 0.0 % A 100.0 % B, 47.5 min: 0.0 % A 100.0 % B, 47.6 min: 99.0 % A 1.0 % B, 53.0 min: 99.0 % A 1.0 % B. The recorded DAD signal was set to 260 nm with a bandwidth of 4 nm. The measured mass range (m/z) was 500 u – 3200 u with a scan rate of 1 spectrum/sec. The settings were: sheath gas flow: 11 L/min, sheath gas temperature: 400°C, nebulizer: 45 psig, gas flow: 8 L/min, gas temperature: 325°C, octupole RF-peak: 750 V, skimmer: 65 V, fragmentor: 175 V, nozzle: 2000 V, V-cap: 3500 V. The reference masses were 601.978977 u, 1033.988109 u and 1333.968947 u (commercially available from Agilent).

Finite Element Simulation In order to investigate the effect of thermal non-equilibria, i.e. temperature gradients due to heat flows on a system, we used a 2-dimensional finite element simulation (COMSOL Multiphysics 5.4). There we simulated the heat transfer, the convection of the bulk liquid, and the transport of the diluted species in the thermal gradient of our pores and coupled it to the different polymerization kinetics via rate equations of the concentration (SI-Section IX).

Author Contributions

CFD conceived the study, conducted the experiments, analyzed the data, ran the simulations and wrote the manuscript. AI gave major input to presenting the data and to writing the manuscript. DT helped to analyze the data for Figs. 1 and 2 and wrote parts of the Supplementary Information. TM provided the setup for the experiments for Fig. 3, conducted experiments and helped to write the manuscript. RMQ helped to analyze the data for Fig. 3. CBM played a decisive role in the development of the experimental technique. DB conceived the study, guided the experimental progress, coded the LabVIEW analysis programs and supervised the project.

Conflicts of interest

There are no conflicts to declare.

Notes and references

1   Gilbert W. The RNA world. Nature. 1986;319,618.
2   Powner M, Gerland B, Sutherland J. Synthesis of activated pyrimidine ribonucleotides in prebiotically plausible conditions. Nature. 2009;459,239–242.
3   Becker S, Feldmann J, Wiedemann S, Okamura H, Schneider C, Iwan K, Crisp A, Rossa M, Amatov T, Carell T. Unified prebiotically plausible synthesis of pyrimidine and purine RNA ribonucleotides. Science. 2019;366(6461),76-82.
4   Teichert JS, Kruse FM, Trapp O. Direct Prebiotic Pathway to DNA Nucleosides. Angew Chem Int Ed. 2019;58,9944.
5   Ritson DJ, Sutherland JD. Conversion of biosynthetic precursors of RNA to those of DNA by photoredox chemistry. J Mol Evol. 2014;78(5):245-50.
6   Steer AM, Bia N, Smith DK, Clarke PA. Prebiotic synthesis of 2-deoxy-d-ribose from interstellar building blocks promoted by amino esters or amino nitriles. Chem Commun. 2017;53,10362–10365.
7   Jauker M, Griesser H, Richert C. Spontaneous Formation of RNA Strands, Peptidyl RNA, and Cofactors. Angew Chem Int Ed Engl. 2015;54(48):14564-14569.
8   Ertem G, Ferris JP. Synthesis of RNA oligomers on heterogeneous templates. Nature. 1996;379(6562):238-40.
9   Verlander MS, Lohrmann R, Orgel LE. Catalysts for the self-polymerization of adenosine cyclic 2', 3'-phosphate. Journal of molecular evolution. 1973;2(4),303–316.
10 Lohrmann R, Orgel L. Prebiotic Activation Processes. Nature. 1973;244,418–420.
11 Ertem G, Ferris J. Synthesis of RNA oligomers on heterogeneous templates. Nature. 1996;379,238–240.
12 Burcar BT, Jawed M, Shah H, McGown LB. In Situ Imidazole Activation of Ribonucleotides for Abiotic RNA Oligomerization Reactions. Orig Life Evol Biosph. 2015;45,31–40.
13 Kricheldorf HR. Leben durch chemische Evolution. Springer. 2019;pp.135-141.

14 Dass AV, Wunnava S, Langlais J, von der Esch B, Krusche M, Ufer L, Chrisam N, Dubini R, Gartner F, Angerpointner S, Dirscherl CF, Rovó P, Mast CB, Šponer JE, Ochsenfeld C, Frey E, Braun D. RNA Oligomerisation without Added Catalyst from 2',3'-cyclic Nucleotides by Drying at Air-Water Interfaces. ChemSystemsChem. 2022;e202200026.
15 Verlander MS, Orgel LE. Analysis of High Molecular Weight Material from the Polymerization of Adenosine Cyclic 2', 3'-Phosphate. J Mol Evol. 1974;3(2),115–120.
16 Morasch M, Mast CB, Langer JK, Schilcher P, Braun D. Dry Polymerization of 3',5'-Cyclic GMP to Long Strands of RNA. Chem Bio Chem. 2014;15(6),879–883.
17 Šponer JE, Šponer J, Giorgi A, Di Mauro E, Pino S, Costanzo G. Untemplated Nonenzymatic Polymerization of 3',5'cGMP: A Plausible Route to 3',5'-Linked Oligonucleotides in Primordia. J Phys Chem B. 2015;119(7),2979–2989.
18 O'Flaherty DK, Kamat NP, Mirza FN, Li L, Prywes N, Szostak JW. Copying of Mixed-Sequence RNA Templates inside Model Protocells. J Am Chem Soc. 2018;140,15,5171–5178.
19 Peng H, Lelievre A, Landenfeld K, Müller S, Chen IA. Vesicle encapsulation stabilizes intermolecular association and structure formation of functional RNA and DNA. Current Biology. 2022;32,1,86-96,e6.
20 Moore W , Webb A. Heat-pipe Earth. Nature. 2013;501,501–505.
21 Kelley DS, Karson JA, Früh-Green GL, Yoerger DR, Shank TM, Butterfield DA, Hayes JM, Schrenk MO, Olson EJ, Proskurowski G, Jakuba M, Bradley A, Larson B, Ludwig K, Glickson D , Buckman K, Bradley AS, Brazelton WJ, Roe K, Elend MJ, Delacour A, Bernasconi SM, Lilley MD, Baross JA, Summons RE, Sylva SP. A serpentinite-hosted ecosystem: the Lost City hydrothermal field. Science. 2005;307(5714):1428-1434.
22 Mast CB, Schink S, Gerland U, Braun D. Escalation of polymerization in a thermal gradient. Proc Natl Acad Sci USA. 2013;110(20):8030-8035.
23 Budin I, Bruckner RJ, Szostak JW. Formation of Protocell-like Vesicles in a Thermal Diffusion Column. J Am Chem Soc. 2009;131,28,9628–9629.
24 Niether D, Afanasenkau D, Dhont JKG, Wiegand S. Accumulation of formamide in hydrothermal pores to form prebiotic nucleobases. Proc Natl Acad Sci USA. 2016;113(16).
25 Mast CB, Braun D. Thermal Trap for DNA Replication. Phys Rev Lett. 2010;104,188102.
26 Kreysing M, Keil L, Lanzmich S, Braun D. Heat flux across an open pore enables the continuous replication and selection of oligonucleotides towards increasing length. Nat Chem. 2015;7(3):203-208.
27 Keil L, Hartmann M, Lanzmich S, Braun D. Probing of molecular replication and accumulation in shallow heat gradients through numerical simulations. Phys Chem Chem Phys. 2016;18,20153-20159.
28 Baaske P, Weinert FM, Duhr S, Lemke KH, Russell MJ, Braun D. Extreme accumulation of nucleotides in simulated hydrothermal pore systems. Proc Natl Acad Sci USA. 2007;104,9346–9351.
29 Wang Z, Kriegs H, Wiegand S. Thermal Diffusion of Nucleotides. J Phys Chem B. 2012;116,25,7463–7469.
30 Edeleva E, Salditt A, Stamp J, Schwintek P, Boekhoven J, Braun D. Continuous nonenzymatic cross-replication of DNA strands with in situ activated DNA oligonucleotides. Chem Sci. 2019;10,5807-5814.
31 Morasch M, Liu J, Dirscherl CF, Ianeselli A, Kühnlein A, Le Vay K, Schwintek P, Islam S, Corpinot MK, Scheu B, Dingwell DB, Schwille P, Mutschler H, Powner MW, Mast CB, Braun D. Heated gas bubbles enrich, crystallize, dry, phosphorylate and encapsulate prebiotic molecules. Nature Chemistry. 2019;11(9):779-788.

32 Ianeselli A, Mast CB and Braun D. Periodic Melting of Oligonucleotides by Oscillating Salt Concentrations triggered by Microscale Water Cycles inside Heated Rock Pores. Angewandte Chemie. 2019;131,37:13289-13294.

33 Waring RH, Running SW. Forest Ecosystems: Analysis at Multiple Scales. Academic Press. 2007;pp.19–57.

34 Toner JD, Catling DC. A carbonate-rich lake solution to the phosphate problem of the origin of life. Proc Natl Acad Sci USA. 2019;117(2).

35 Damer B, Deamer D. The Hot Spring Hypothesis for an Origin of Life. Astrobiology. 2020;20:4,429-452.

36 Benison KC, Bowen BB. Extreme sulfur-cycling in acid brine lake environments of Western Australia. Chemical Geology. 2013;351,154-167.

37 Mungi CV, Rajamani S. Characterization of RNA-Like Oligomers from Lipid-Assisted Nonenzymatic Synthesis: Implications for Origin of Informational Molecules on Early Earth. Life. 2015;5(1),65-84.

38 Dose K. Peptides and amino acids in the primordial hydrosphere. Biosystems. 1975;6(4):224-228.

39 De Duve C, De Neufville R. Blueprint for a cell: the nature and origin of life. Carolina Biological Supply Company Burlington NC. 1991.

40 Reichl M, Herzog M, Götz A, Braun D. Why charged molecules move across a temperature gradient: the role of electric fields. Physical Review Letters. 2014;112,198101.

41 Duhr S, Braun D. Why molecules move along a temperature gradient. Proc Natl Acad Sci USA. 2006;103,19678–19682.

42 Debye P. Zur Theorie des Clusiusschen Trennungsverfahrens. Ann Phys Leipzig. 1939;428,284-294.

43 Clusius K, Dickel G. Neues Verfahren zur Gasentmischung und Isotopentrennung. Naturwissenschaften. 1938;26,546.

44 Salditt A, Keil LMR, Horning DP, Mast CB, Joyce GF, Braun D. Thermal Habitat for RNA Amplification and Accumulation. Physical Review Letters. 2020;125,048104.

45 Reichl M, Herzog M, Greiss F, Wolff M, Braun D. Understanding the similarity in thermophoresis between single- and double-stranded DNA or RNA. Physical Review E. 2015;91,062709.

46 Ferris JP, Kamaluddin A. Oligomerization reactions of deoxyribonucleotides on montmorillonite clay: the effect of mononucleotide structure on phosphodiester bond formation. Orig Life Evol Biosph. 1989;19:609-619.

47 Burcar BT, Barge LM, Trail D, Watson EB, Russell MJ, McGown LB. RNA Oligomerization in Laboratory Analogues of Alkaline Hydrothermal Vent Systems. Astrobiology. 2015;15(7):509-22.

48 Anderson BA, Krishnamurthy R. Heterogeneous Pyrophosphate-Linked DNA-Oligonucleotides: Aversion to DNA but Affinity for RNA. Chem Eur J. 2018;24,6837.

49 Ianeselli A, Atienza M, Kudella P, Mast CB, Gerland U, Braun D. Water cycles in a Hadean CO2 atmosphere drive the evolution of long DNA. Nature Physics. 2022;18:579–585.

50 Deegan RD, Bakajin O, Dupont TF, Huber G, Nagel SR, Witten TA. Capillary flow as the cause of ring stains from dried liquid drops. Nature. 1997;389:827–829.

51 Hu H, Larson RG. Evaporation of a Sessile Droplet on a Substrate. J Phys Chem B. 2002;106,6,1334–1344.

52 Matreux T, Le Vay K, Schmid A, Aikkila P, Belohlavek L, Çalışkanoğlu AL, Salibi E, Kühnlein A, Springsklee C, Scheu B, Dingwell DB, Braun D, Mutschler H, Mast CB. Heat flows in rock cracks naturally optimize salt compositions for ribozymes. Nat Chem. 2021;13:1038–1045.

53 Engelhart AE, Powner MW, Szostak JW, Nat Chem. 2013;5,390–394.

54 Sheng J, Li L, Engelhart AE, Gan J, Wang J, Szostak JW. Proc Natl Acad Sci. 2014;111,3050–3055.

55 Bhowmik S, Krishnamurthy R. Nat Chem. 2019;11:1009–1018.

56 Mariani A, Sutherland JD. Angew Chem Int Ed. 2017;56:6563–6566.

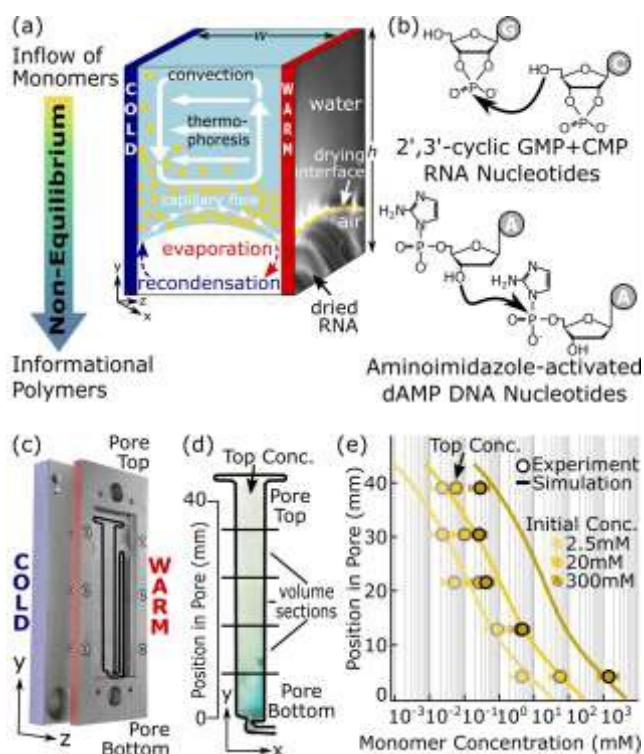## Figures

Figure 1.

FIG. 1. A primordial non-equilibrium habitat accumulates nucleotides and promotes their polymerization. (a) Activated nucleotides are accumulated and polymerized by the superposition of heat-flow driven convection of water and thermophoresis of molecules in a water-filled pore subjected to a thermal gradient. The accumulation of monomers at the bottom of the pore should enable improved polymerization by the enhanced concentration and would retain the products over long times. (b) For polymerization, either aminoimidazole-activated DNA monomers or 2',3'-cyclic RNA monomers were used. (c) To experimentally implement this non-equilibrium setting a microfluidic structure from a Teflon foil with 170 μm width are sandwiched between two thermally conducting sapphire plates. The pore is filled with sample and cooling and heating are applied (SI-Section II). (d) Accumulation is visualized by the co-accumulation of fluorescent Cy5 for 24 h in a thermal of 8°C to 30°C across a 170 μm thin sapphire chamber (170 μm × 7 mm × 40 mm, total volume: 62 μl). Horizontal lines indicate the volume partitions extracted for analysis after accumulation and fast freezing. (e) After 24 h, the accumulation of non-activated nucleotides spreads over four orders of magnitude along the pore height (circles). This accumulation is independent of the initial starting concentrations of 2.5, 20 or 300 mM dAMP and is confirmed by a simulation of fluid flow and thermophoresis (lines). Already after the 24h, the fit reveals a relative accumulation over more than four orders of magnitude. Error bars indicate a ± 50 % error, taken from triplicates on representative experiments (see SI-section VIII.2).

Figure 2.
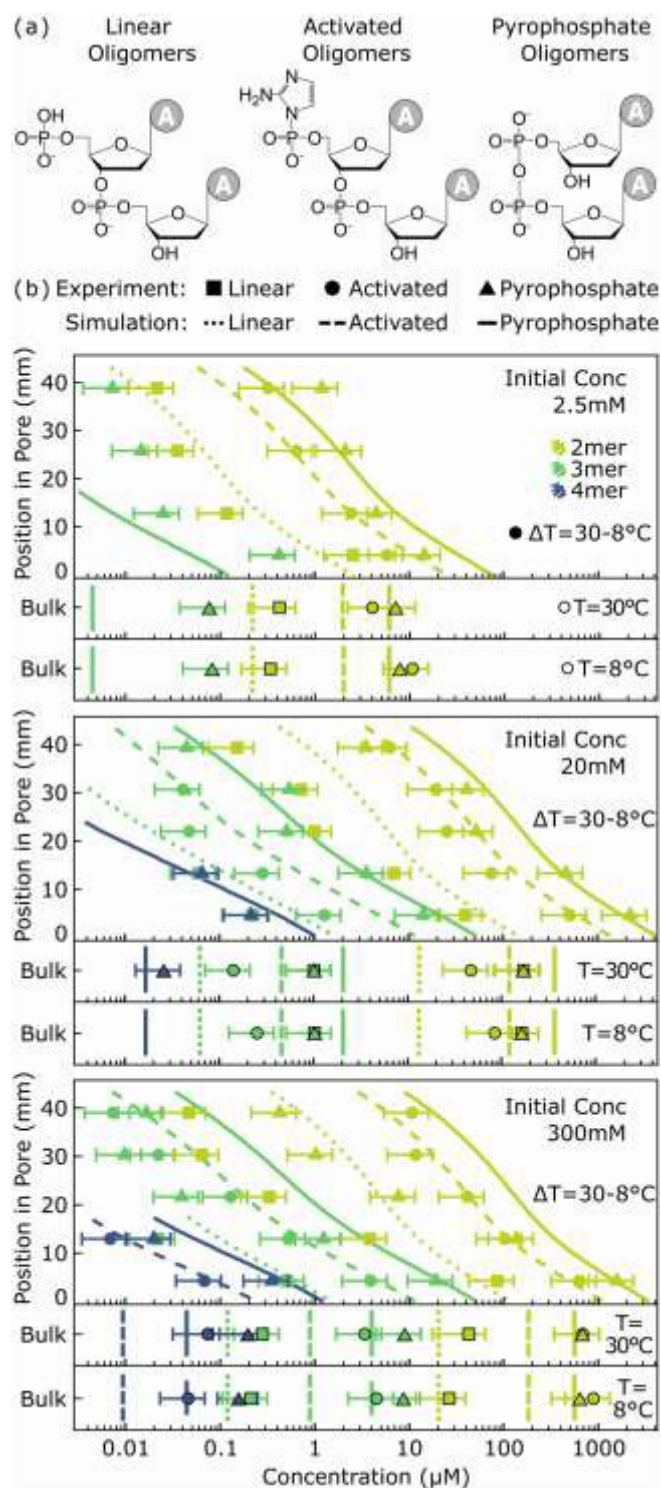
FIG. 2. Enhanced DNA polymerization in a thermal gradient.
(a) Polymerization from aminoimidazole-activated dAMP monomers produces linear, activated and pyrophosphate oligomers, analyzed by HPLC and ESI-TOF mass spectrometry. (b) Heat-flow enhanced DNA polymerization in a thermophoretic pore at a temperature gradient of ΔT = 8°C – 30°C = 22°C formed up to 4mers after 24 h (markers). At the pore bottom, the polymerization concentration was 2- to 6-fold higher for the single lengths and oligomer types than in the control reaction at isothermal bulk conditions (SI-Figs. 14 and 16). This experimental result is supported by finite element calculations of fluid flow, thermophoresis and polymerization kinetics (lines). A range of initial concentrations were tested. Error bars indicate a ± 50 % error, taken from triplicates on representative polymerization experiments (see SI-section VIII.2).
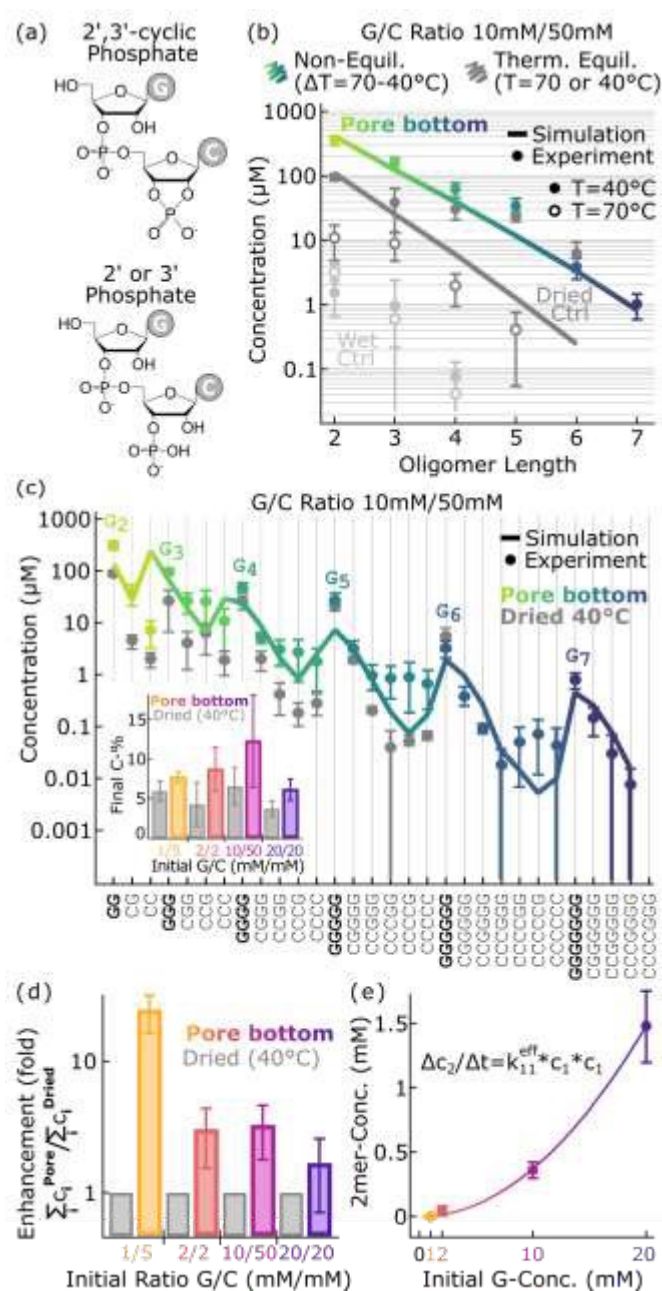
ARTICLE

Journal Name

Figure 3.

FIG. 3. Thermogravitational accumulation and with interfacial drying drives RNA polymerization. (a) The polymerization from 2',3'-cyclic RNA monomers yields oligomers that are still activated with a 2',3'-cyclic phosphate or have inactivated endings with a phosphate at 2' or 3'. (b) Polymerization of 10 mM 2',3'-cGMP and 50 mM 2',3'-cCMP is enhanced in the thermal gradient setting $\Delta T = 70°C - 40°C = 30°C$ (colored circles). Polymer concentrations and lengths from the pore exceed reactions in the dry (dark grey circles) or the bulk at isothermal conditions (light grey circles). Notably, polymerization was enhanced although only triggered at the pore bottom where continuous wet-dry cycles at the air bubble were hosting the polymerization. Finite element simulation of fluid flow, thermophoresis and polymerization confirmed both the length distribution and the enhancement of thermophoretic trapping (lines). The polymerization was captured in the model using a reduced dimer on-rate $k_{11} = k_{on}/60 = 15.8 * 10^{-6} (Ms)^{-1}$ (see SI-Table S5) and estimating the hydrolysis of 2',3'-cyclic phosphate to the inactive 2' or 3' phosphate with $k_{off} = 1/day$, both motivated by the results of the same reaction in the dry state[14]. All error bars indicate the standard deviations of the mean from the triplicate experiment. (c) HPLC/ESI-TOF mass spectra were fitted and calibrated to determine the base compositions of the formed oligomers (colored circles). The base G dominates the polymer products. The finite element model rationalized the polymerization characteristics by differential kon rates k_{GG}, k_{GC} and k_{CC} (solid line). In the thermal trap, C is incorporated more readily into the strands as compared to pure drying conditions (grey circles) independently for all tested initial monomer compositions and concentrations (also see SI-Fig. 15). Inset: The thermal pore increases the formation of mixed sequences and up to doubles the rate of incorporation of C-nucleotides for all tested initial monomer compositions and concentrations. (d) The concentration of oligomers at the pore bottom surmounts dry polymerization especially for the lowest initial G-concentration, indicating a nonlinear boost from the accumulation. (e) As expected for the rate limiting step of dimer formation, we find a quadratic dependency on the G-monomer initial concentration. We fitted an effective dimer formation rate that includes the accumulation effects of the crack with $k_{11}^{eff} = 5.7 \pm 0.1 * 10^{-5} (Ms)^{-1}$, around order of magnitude higher than what is needed to fit the polymerization in the microscopic model of Figure 3c (main figure). This enhancement confirms in a nutshell the enhancing effect of the heated crack.
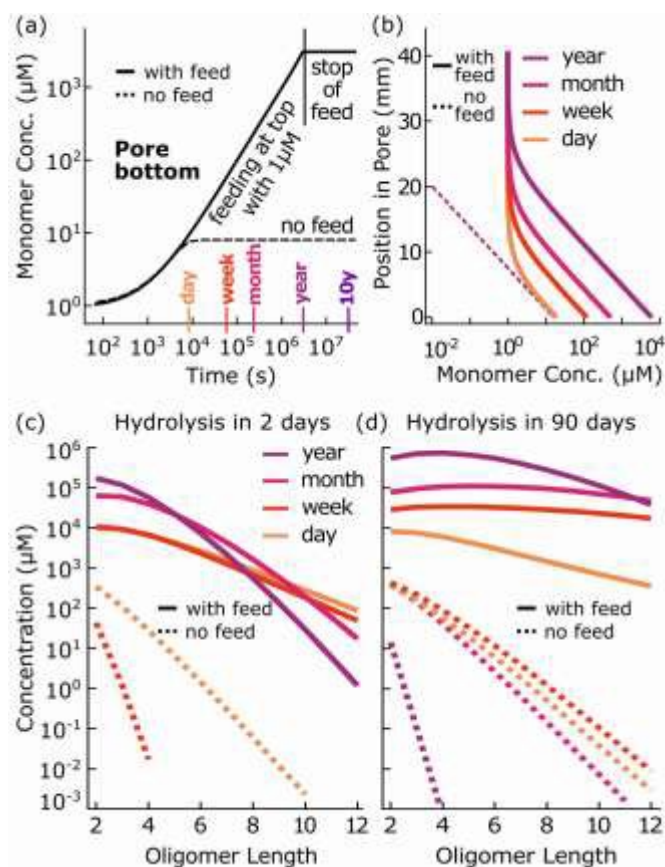
Journal Name

ARTICLE

Figure 4.

FIG. 4. **Heated pores enable feeding without dilution.** We used simulations to explore the long term behaviour of polymerization and accumulation in a heated crack. (a) Monomer feeding of a thermal pore was implemented by setting the monomer concentration at the top to a moderate value of 1µM and allowing convection and thermophoresis to transport the monomers into the trap using a full 2D simulation. The low concentration of the feeding makes it slow, but persistent, reaching bottom monomer concentrations of more than $10^4 \times 1$ µM after a year (solid line). Interestingly, the accumulation is so strong in our setting that no molecules are expected to leave the pore after the feeding stops. In the long run under continuous heating, the whole volume of the pore will be filled with a theoretical concentration ratio of $c_{bottom}/c_{top}=10^6$. (b) A closed pore reaches a steady state after one day (broken line), however an open pore can accumulate the low monomer concentration to its bottom and fills itself up over the course of years (solid lines; SI-Section IX). In our experiment, the concentration at the pore bottom was raised at the expense of a concentration depletion at its top and no further accumulation at the bottom (broken line). (c,d) To explore how this feeding will be able to counterbalance hydrolysis, we modelled the RNA polymerization from 2',3'-cyclic monomers using a 0D model with explicit G-C mixed sequences up to 21mers with adjusted polymerization rates to emulate the 2D pore kinetics of Figure 3c. The feeding was mimicked with an inflow of 2',3'-cyclic monomers at a concentration of 0.6 µM/s as inferred from the 2D simulation in (a). For a closed reaction without feeding, polymers are eventually lost by stopping the polymerization due to the deactivation of the active 2',3'-cyclic phosphate end with $k_{off} = 1/day$, leading to passive molecules not being able to re-polymerize which are eventually hydrolysed to shorter strands with a rate of (c) 1/(2 days) or (d) 1/(90 days), shown as broken lines. The feeding of the crack with a moderate 1µM concentration of active monomers from the top could therefore compensate even strong hydrolysis, creating RNA with long lengths and high concentrations at the bottom of the crack (solid lines). The hydrolysis rates were chosen to mimic worst case hydrolysis at the given low salt concentrations for (c) single and (d) double stranded RNA.